2.6 PIEZOELECTRIC SENSORS

Piezoelectric sensors are used to measure physiological displacements and record heart sounds. Piezoelectric materials generate an electric potential when mechanically strained, and conversely an electric potential can cause physical deformation of the material. The principle of operation is that when an asymmetrical crystal lattice is distorted, a charge reorientation takes place, causing a relative displacement of negative and positive charges. The displaced internal charges induce surface charges of opposite polarity on opposite sides of the crystal. Surface charge can be determined by measuring the difference in voltage between electrodes attached to the surfaces.

Initially, we assume infinite leakage resistance. Then, the total induced charge q is directly proportional to the applied force f.

$$q = kf \tag{2.13}$$

where k is the piezoelectric constant, C/N. The change in voltage can be found by assuming that the system acts like a parallel-plate capacitor where the voltage v across the capacitor is charge q divided by capacitance C. Then, by substitution of (2.8), we get

$$v = \frac{kf}{C} = \frac{kfx}{\varepsilon_0 \varepsilon_r A} \tag{2.14}$$

Tables of piezoelectric constants are given in the literature (Lion, 1959; and Cobbold, 1974).

Typical values for k are 2.3 pC/N for quartz and 140 pC/N for barium titanate. For a piezoelectric sensor of 1 cm^2 area and 1 mm thickness with an applied force due to a 10 g weight, the output voltage v is 0.23 mV and 14 mV for the quartz and barium titanate crystals, respectively.

There are various modes of operation of piezoelectric sensors, depending on the material and the crystallographic orientation of the plate (Lion, 1959). These modes include the thickness or longitudinal compression, transversal compression, thickness-shear action, and face-shear action.

Also available are piezoelectric polymeric films, such as polyvinylidene fluoride (PVDF) (Hennig, 1988; Webster, 1988). These films are very thin, lightweight and pliant, and they can be cut easily and adapted to uneven surfaces. The low mechanical quality factor does not permit resonance applications, but it permits acoustical broadband applications for microphones and loudspeakers.

Piezoelectric materials have a high but finite resistance. As a consequence, if a static deflection x is applied, the charge leaks through the leakage resistor (on the order of 100 GΩ). It is obviously quite important that the input impedance of the external voltage-measuring device be an order of magnitude higher than that of the piezoelectric sensor. It would be helpful to look at the

field are described by vectors which specify the sense of direction. If a mechanical stress is to produce an electric polarization, a directional quality must therefore be inherent in the body. Conversely, in an isotropic material (i.e., a body without inherent directional quality) mechanical stress or strain caused by an electric field must be equal for opposite directions of the field; this implies a quadratic dependence on the field. This quadratic effect, known as electrostriction , is substantial only in materials of very high dielectric constant, notably ferroelectric materials. A necessary condition for the occurrence of the piezoelectric effect, including the converse linear dependence of stress or strain on electric field, is the absence of a centre of symmetry. Twenty-one of the 32 crystal symmetry classes (see CRYSTALLOGRAPHY) lack this symmetry element, and crystals in all but one of these classes can exhibit piezoelectricity. A qualitative test for presence of piezoelectricity is therefore useful in crystal structure determination. Piezoelectricity has been observed by qualitative tests in about 1,000 crystal species, while more or less complete quantitative data have been taken on about 100 crystals. Sulfates, phosphates, tartrates and various sugars and their derivatives contribute heavily to the latter number. The combination of symmetry planes and axes that is characteristic of any crystal class determines which components of stress and of electric polarization may be linked by piezoelectricity. It must be emphasized, however, that crystallographic symmetry merely states what effects are forbidden; the magnitude of the allowed effects is a matter of empirical observation or of calculation from atomic structure and atomic dynamics. While some principles of such calculations were outlined as early as 1920, the quantitative data available by the early 1960s were almost entirely derived from measurements.

A Molecular Model – Symmetry as well as the molecular approach can be illustrated by the simplest crystal structure capable of piezoelectricity. This is the cubic modification of zinc sulfide, ZnS, known as sphalerite or zinc blende. A unit cell of this structure is shown in fig. 1. It contains only two different atoms, each atom of one kind surrounded by four atoms of the other kind placed at the corners of a tetrahedron. The symmetry class is 43m in the international designation. Compressional stress (stress – force per unit area) applied parallel to an edge of the unit cell will not produce an electric moment since the sulfur atoms (negative) lie in planes halfway between the zinc atoms (positive), and there is nothing in the nature of the applied stress to disturb this symmetry. If, however, a shearing stress is applied in the horizontal plane, resulting in the shearing strain (displacement per unit length) indicated by long horizontal arrows in fig. 1, then tetrahedral symmetry of the four zinc atoms around each sulfur atom (and vice versa) is disturbed and the sulfur atom is displaced toward the two zinc atoms which have moved apart. The amount of displacement is calculated readily if one postulates that the distance between nearest neighbour atoms remains constant. For a shearing strain of 1/1000 (angle of distortion about 1/20°) the displacement of the sulfur atoms against the zinc atoms in the direction perpendicular to the plane of the shear is 1/4000 of the unit cell dimension. The resulting electric polarization is the product of this displacement with the number of sulfur atoms per unit volume and the electric charge per atom. To obtain agreement with the observed piezoelectric effect it is necessary to place a negative charge of one-fourth of an electron on the sulfur and the same positive charge on the zinc. This is in accord with the partially polar character of zinc sulfide. A quantitative theory would have to consider also the distribution of electric charge within each atom.

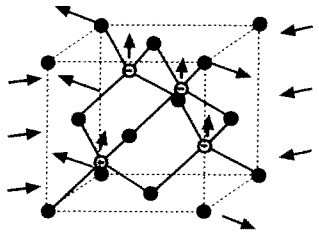

Fig 1 – Unit cell of cubic zinc sulfide crystal with positive zinc and negative sulfur atoms. Long horizontal arrows indicate applied shearing strain, short vertical arrows the internal electric charge displacement linked to this strain.

Piezoelectricity in Various Crystal Classes – in zinc sulfide and all other piezoelectric crystals of cubic symmetry, the piezo electric effect of any mechanical stress can be expressed in terms of the single piezoelectric constant relating electric polarization parallel to a cubic axis to strain in the plane perpendicular to this axis. In crystals of lower symmetry, a number of independent piezoelectric constants are needed to describe all possible piezo electric effects. For the triclinic asymmetric crystal class there are 18 independent coefficients. Fortunately, the most important piezoelectric crystals belong to classes having several symmetry elements, and are characterized by only two or three piezoelectric constants. If, starting from class 43m, one of the three axes is made different from the other two, the tetragonal crystal class 42m results, of which ammonium dihydrogen phosphate is an important example. This class has two independent piezoelectric constants. If all three axes are different, the orthorhombic crystal class 22, which includes Rochelle salt, is obtained. The trigonal crystal system includes two very important piezo electric crystals, quartz and tourmaline. The former has three twofold axes of symmetry in addition to the threefold, principal axis; the crystal class is 32, characterized by two piezoelectric constants, one relating compressional stress parallel to a twofold axis with an electric polarization in the same direction, while the second constant relates shearing stress in the plane perpendicular to a twofold axis with polarization parallel to that axis. Tourmaline line, crystal class 3m, has three planes of symmetry intersecting in the threefold axis. Its most important piezoelectric constant relates polarization parallel to this axis to compressional stress in the same direction. It is in the general nature of stress and strain (see ELASTICITY) that a shearing stress or strain can

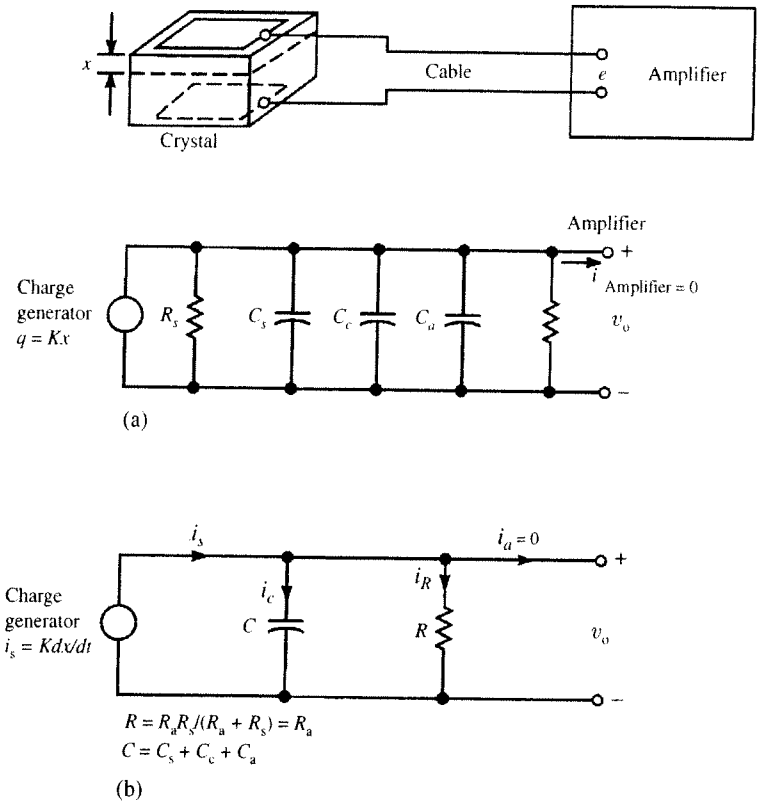

Figure 2.10 (a) Equivalent circuit of piezoelectric sensor, where R_s = sensor leakage resistance, C_s = sensor capacitance, C_c = cable capacitance, C_a = amplifier input capacitance, R_a = amplifier input resistance, and q = charge generator. (b) Modified equivalent circuit with current generator replacing charge generator. (From *Measurement Systems: Application and Design*, by E. O. Doebelin. Copyright © 1990 by McGraw-Hill, Inc. Used with permission of McGraw-Hill Book Co.)

equivalent circuit for the piezoelectric sensor [Figure 2.10(a)] in order to quantify its dynamic-response characteristics.

This circuit has a charge generator q defined by

$$q = Kx \tag{2.15}$$

where where

K = proportionality constant, C/m

x = deflection

The circuit may be simplified by converting the charge generator to a current generator, i_s.

$$i_s = \frac{dq}{dt} = K\frac{dx}{dt} \tag{2.16}$$

The modified circuit is shown in Figure 2.10(b), where the resistances and capacitances have been combined. Assuming that the amplifier does not draw any current, we then have

$$i_s = i_C + i_R \tag{2.17}$$

$$v_o = v_C = \left(\frac{1}{C}\right)\int i_C dt \tag{2.18}$$

$$i_s - i_R = C\left(\frac{dv_o}{dt}\right) = K\frac{dx}{dt} - \frac{v_o}{R} \tag{2.19}$$

or

$$\frac{V_o(j\omega)}{X(j\omega)} = \frac{K_s j\omega\tau}{j\omega\tau + 1} \tag{2.20}$$

where

$K_s = K/C$ (sensitivity, V/m)

$\tau = RC$ (time constant)

EXAMPLE 2.2 A piezoelectric sensor has $C = 500$ pF. The sensor leakage resistance is 10 GΩ. The amplifier input impedance is 5 MΩ. What is the low-corner frequency?

ANSWER We may use the modified equivalent circuit of the piezoelectric sensor given in Figure 2.10(b) for this calculation.

$$f_c = 1/(2\pi RC) = 1/[2\pi(5 \times 10^6)(500 \times 10^{-12})] = 64 \text{ Hz}$$

Note that by increasing the input impedance of the amplifier by a factor of 100, we can lower the low-corner frequency to 0.64 Hz.

EXAMPLE 2.3 For a piezoelectric sensor plus cable that has 1 nF capacitance, design a *voltage amplifier* (not a charge amplifier) by using only *one* noninverting amplifier that has a gain of 10. It should handle a charge of 1 μC generated by the carotid pulse without saturation. It should not drift into saturation because of bias currents. It should have a frequency response from 0.05 to 100 Hz. Add the minimal number of extra components to achieve the design specifications.

ANSWER Calculate the voltage from $V = Q/C = 1\,\mu\text{C}/1\,\text{nF} = 1\,\text{kV}$. Because this is too high, add a shunt capacitor $C_s = 1\,\mu\text{F}$ to achieve 1.0 V. Allow for a gain of 10. To achieve low-corner frequency, add shunt

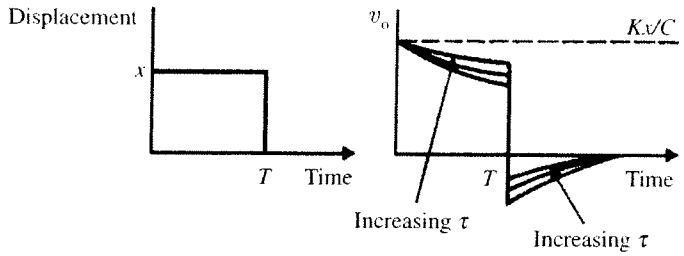

Figure 2.11 Sensor response to a step displacement (From Doebelin, E. O. 1990. *Measurement Systems: Application and Design*, New York: McGraw-Hill.)

$R_s = 1/2\pi f_c C = 1/2\pi(0.05)(1\,\mu\text{F}) = 3.2\ \text{M}\Omega$. To achieve gain of +10 in a noninverting amplifier, select $R_f = 10\,\text{k}\Omega$ and $R_i = 11.1\,\text{k}\Omega$. To achieve high-corner frequency, $C_f = 1/2\pi f_c R_f = 1/2\pi(100)(10\,\text{k}\Omega) = 160\,\text{nF}$.

Figure 2.11 shows the voltage-output response of a piezoelectric sensor to a step displacement x. The output decays exponentially because of the finite internal resistance of the piezoelectric material. At time equal to T the force is released, and a displacement restoration results that is equal to and opposite of the original displacement. This causes a sudden decrease in voltage of magnitude Kx/C, with a resulting undershoot equal to the decay prior to the release of the displacement. The decay and undershoot can be minimized by increasing the time constant, $\tau = RC$. The simplest approach to increasing τ is to add a parallel capacitor. However, doing so reduces the sensitivity in the midband frequencies according to (2.20).

Another approach to improving the low-frequency response is to use the charge amplifier described in Section 3.8.

Because of its mechanical resonance, the high-frequency equivalent circuit for a piezoelectric sensor is complex. This effect can be represented by adding a series RLC circuit in parallel with the sensor capacitance and leakage resistance. Figure 2.12 shows the high-frequency equivalent circuit and its frequency response. Note that in some applications—for example, in the case of crystal filters—the mechanical resonance is useful for accurate frequency control.

Piezoelectric sensors are used quite extensively in cardiology for external (body-surface) and internal (intracardiac) phonocardiography. They are also used in the detection of Korotkoff sounds in blood-pressure measurements (Chapter 7). Additional applications of piezoelectric sensors involve their use in measurements of physiological accelerations. A piezoelectric sensor and circuit can measure the acceleration due to human movements and provide an estimate of energy expenditure (Servais *et al.*, 1984). Section 8.4 describes ultrasonic blood-flow meters in which the piezoelectric element operating at mechanical resonance emits and senses high-frequency sounds. Li and Su (2006) describe piezoelectric sensors as sensitive mass sensors to detect and measure a broad variety of biomedical analytes in both gas and liquid phases based on the adsorption and/or desorption of target analyte(s) on the sensor surface.

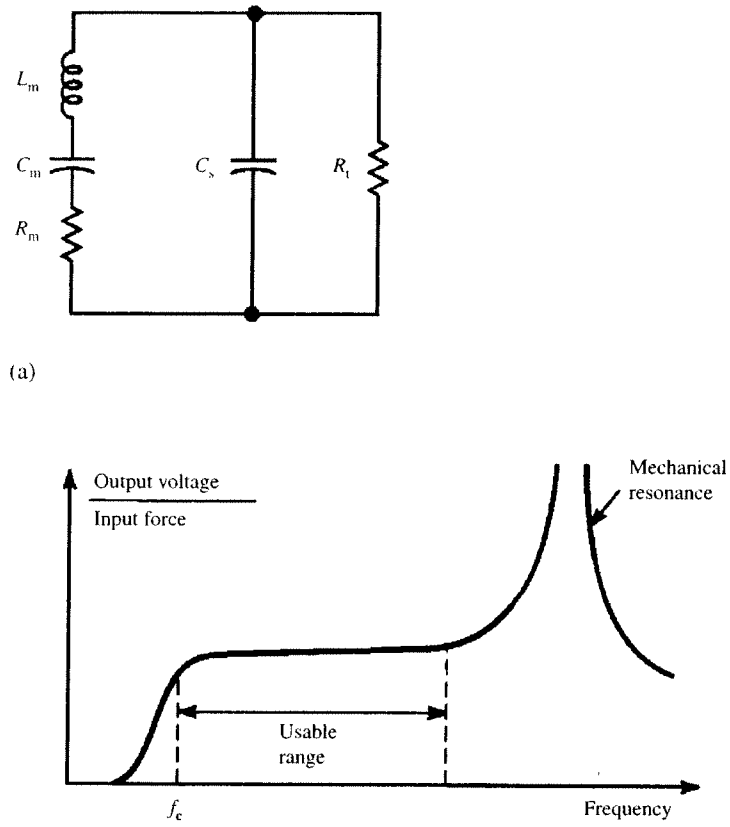

Figure 2.12 (a) High-frequency circuit model for piezoelectric sensor. R_s is the sensor leakage resistance and C_s is the capacitance. L_m, C_m, and R_m represent the mechanical system, (b) Piezoelectric sensor frequency response. (From *Transducers for Biomedical Measurements: Principles and Applications*, by R. S. C. Cobbold. Copyright (c) 1974, John Wiley and Sons, Inc. Reprinted by permission of John Wiley and Sons, Inc.)

2.7 TEMPERATURE MEASUREMENTS

A patient's body temperature gives the physician important information about the physiological state of the individual. External body temperature is one of many parameters used to evaluate patients in shock, because the reduced blood pressure of a person in circulatory shock results in low blood flow to the periphery. A drop in the big-toe temperature is a good early clinical warning of shock. Infections, on the other hand, are usually reflected by an increase in body temperature, with a hot, flushed skin and loss of fluids. Increased ventilation, perspiration, and blood flow to the skin result when high fevers destroy temperature-sensitive enzymes and proteins. Anesthesia decreases body temperature by depressing the thermal regulatory center. In fact, physicians routinely induce hypothermia in surgical cases in which they wish to decrease a patient's metabolic processes and blood circulation.

In pediatrics, special heated incubators are used for stabilizing the body temperature of infants. Accurate monitoring of temperature and regulatory

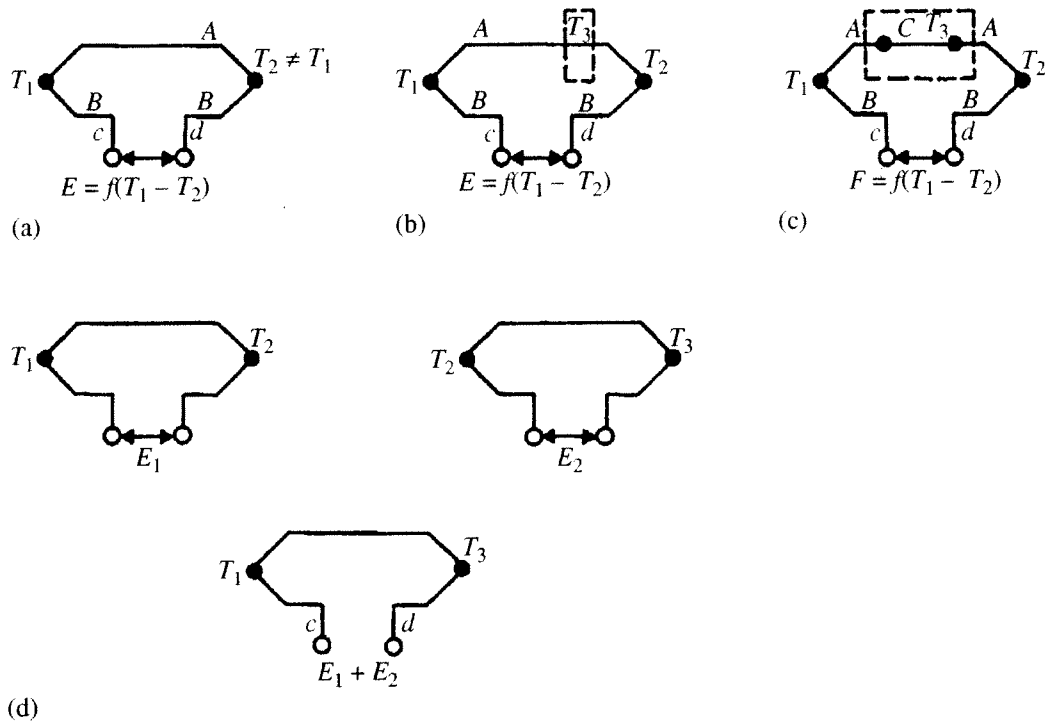

Figure 2.13 Thermocouple circuits (a) Peltier emf, (b) law of homogeneous circuits, (c) law of intermediate metals, (d) law of intermediate temperatures.

An understanding of the three empirical thermocouple laws leads to using them properly. The first law, *homogeneous circuits*, states that in a circuit composed of a single homogeneous metal, one cannot maintain an electric current by the application of heat alone. In Figure 2.13(b), the net emf at *c–d* is the same as in Figure 2.13(a), regardless of the fact that a temperature distribution (T_3) exists along one of the wires (A).

The second law, *intermediate metals*, states that the net emf in a circuit consisting of an interconnection of a number of unlike metals, maintained at the same temperature, is zero. The practical implication of this principle is that lead wires may be attached to the thermocouple without affecting the accuracy of the measured emf, provided that the newly formed junctions are at the same temperature [Figure 2.13(c)].

The third law, successive or *intermediate temperatures*, is illustrated in Figure 2.13(d), where emf E_1 is generated when two dissimilar metals have junctions at temperatures T_1 and T_2 and emf E_2 results for temperatures T_2 and T_3. It follows that an emf $E_1 + E_2$ results at *c–d* when the junctions are at temperatures T_1 and T_3. This principle makes it possible for calibration curves derived for a given reference-junction temperature to be used to determine the calibration curves for another reference temperature.

The *thermoelectric sensitivity* α (also called the *thermoelectric power* or the *Seebeck coefficient*) is found by differentiating (2.21) with respect to T. Then

$$\alpha = \frac{dE}{dT} = a + bT + \cdots \tag{2.22}$$

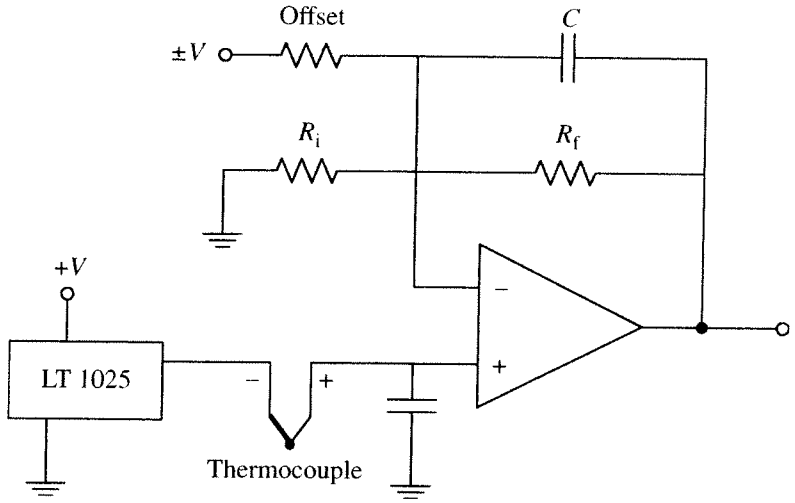

Figure 2.14 The LT1025 electronic cold junction and the hot junction of the thermocouple yield a voltage that is amplified by an inverting amplifier.

Note that α is not a constant but varies (usually increases) with temperature. The sensitivities of common thermocouples range from 6.5 to 80 μV/°C at 20 °C, with accuracies from ¼% to 1%.

For accurate readings, the reference junction should be kept in a triple-point-of-water device the temperature of which is 0.01 ± 0.0005 °C (Doebelin, 1990). Normally the accuracy of a properly constructed ice bath, 0.05 °C with a reproducibility of 0.001 °C is all that is necessary. Temperature-controlled ovens can maintain a reference temperature to within ±0.4 °C. Figure 2.14 shows that modern thermocouple signal conditioners contain an electronic cold junction (Tompkins and Webster, 1988; Sheingold, 1980).

Increased sensitivity may be achieved by connecting a number of thermocouples in series, all of them measuring the same temperature and using the same reference junction. An arrangement of multiple-junction thermocouples is referred to as a *thermopile*. Parallel combinations may be used to measure average temperature.

It is easy to obtain a direct readout of the thermocouple voltage using a digital voltmeter. Chart recordings may be secured by using a self-balancing potentiometer system. The linearity of this latter device is dependent only on the thermocouple and potentiometer; it is independent of the other circuitry.

Thermocouples have the following advantages: fast response time (time constant as small as 1 ms), small size (down to 12 μm diameter), ease of fabrication, and long-term stability. Their disadvantages are small output voltage, low sensitivity, and the need for a reference temperature.

Numerous examples of the use of thermocouples in biomedical research are given in the literature (Wren, 2006). Thermocouples can be made small in size, so they can be inserted into catheters and hypodermic needles.

2.9 THERMISTORS

Thermistors are semiconductors made of ceramic materials that are thermal resistors with a high negative temperature coefficient. These materials react to temperature changes in a way that is opposite to the way metals react to such changes. The resistance of thermistors decreases as temperature increases and increases as temperature decreases (Melo, 2006).

Sapoff (1971) reviewed the various types of thermistors that have been found to be most suitable for biomedical use. The resistivity of thermistor semiconductors used for biomedical applications is between 0.1 and 100 Ω·m.

These devices are small in size (they can be made less than 0.5 mm in diameter), have a relatively large sensitivity to temperature changes (−3 to −5%/°C), and have excellent long-term stability characteristics (±0.2% of nominal resistance value per year).

Figure 2.15(a) shows a typical family of resistance-versus-temperature characteristics of thermistors. These properties are measured for the

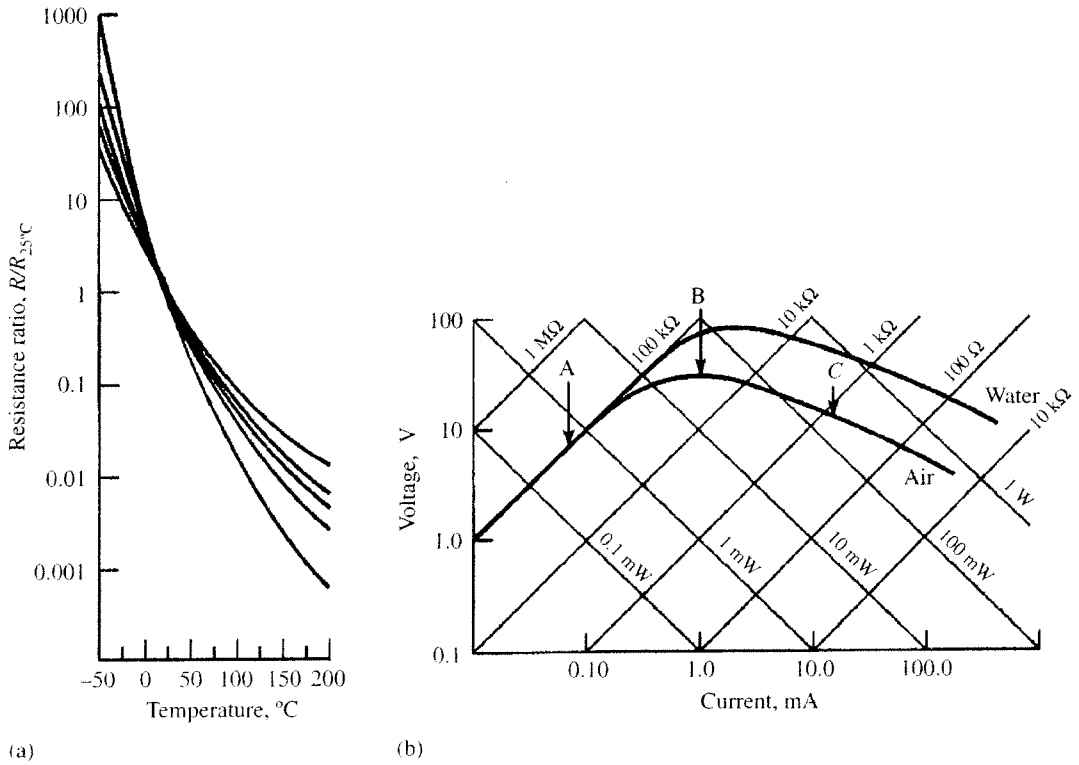

Figure 2.15 (a) Typical thermistor zero-power resistance ratio–temperature characteristics for various materials. (b) Thermistor voltage-versus-current characteristic for a thermistor in air and water. The diagonal lines with a positive slope give linear resistance values and show the degree of thermistor linearity at low currents. The intersection of the thermistor curves and the diagonal lines with negative slope give the device power dissipation. Point *A* is the maximal current value for no appreciable self-heat. Point *B* is the peak voltage. Point *C* is the maximal safe continuous current in air. [Part (b) is from *Thermistor Manual*, EMC-6, © 1974, Fenwal Electronics, Framingham, MA. Used by permission.]

thermistor operated at a very small amount of power such that there is negligible self-heating. This resistance is commonly referred to as *zero-power resistance*. The empirical relationship between the thermistor resistance R_t and absolute temperature T in kelvin (K) (the SI unit *kelvin* does not use a degree sign) is

$$R_t = R_0 e^{[\beta(T_0 - T)/TT_0]} \tag{2.23}$$

where

β = material constant for thermistor, K
T_0 = standard reference temperature, K

The value of β increases slightly with temperature. However, this does not present a problem over the limited temperature spans for biomedical work (10 °C to 20 °C). β, also known as the characteristic temperature, is in the range of 2500 to 5000 K. It is usually about 4000 K.

The temperature coefficient α can be found by differentiating (2.23) with respect to T and dividing by R_t. Thus

$$\alpha = \frac{1}{R_t}\frac{dR_t}{dT} = -\frac{\beta}{T^2}(\%/\text{K}) \tag{2.24}$$

Note from (2.24) that α is a nonlinear function of temperature. This nonlinearity is also reflected in Figure 2.15(a).

The voltage-versus-current characteristics of thermistors, as shown in Figure 2.15(b), are linear up to the point at which self-heating becomes a problem. When there is large self-heating, the thermistor voltage drop decreases as the current increases. This portion of the curve displays a negative-resistance characteristic.

In the linear portion, Ohm's law applies and the current is directly proportional to the applied voltage. The temperature of the thermistor is that of its surroundings. However, at higher currents a point is reached, because of increased current flow, at which the heat generated in the thermistor raises the temperature of the thermistor above ambient. At the peak of the v–i characteristic, the incremental resistance is zero, and for higher currents a negative-resistance relationship occurs. Operations in this region render the device vulnerable to thermal destruction.

Figure 2.15(b) shows the difference in the self-heat regions for a thermistor in water and air due to the differences in thermal resistance of air and water. The principle of variation in thermal resistance can be used to measure blood velocity, as described in Section 8.5.

EXAMPLE 2.4 Sketch typical thermistor v–i characteristics with and without a heat sink. Explain why there is a difference.

ANSWER Figure 2.15(b) shows typical thermistor v–i characteristics in water and air. For low currents Ohm's law applies, and the current is directly proportional to the applied voltage in both cases. The thermistor temperature is close to ambient. The system with water can reach higher current levels and still remain in a linear portion of the v–i curve since the water keeps the thermistor close to ambient temperature. Eventually the thermistor-water combination will self-heat and a negative-resistance relationship will result. In the same manner, the heat sink keeps the thermistor temperature close to ambient at higher current levels and yields characteristics similar to Figure 2.15(b).

EXAMPLE 2.5 For a thermistor assume self-heating $< 0.1\,^{\circ}\text{C}$, voltage $= 5\,\text{V}$, dissipation coefficient (DC) $= 2.0\,\text{mW}/^{\circ}\text{C}$. Calculate minimum thermistor resistance.

ANSWER

$$\Delta T = \frac{P}{\text{D.C.}} = \frac{V^2/R}{\text{D.C.}}$$

$$R = \frac{V^2}{\Delta T(\text{D.C.})} = \frac{5^2}{0.1\,^{\circ}\text{C}(0.002\,\text{W}/^{\circ}\text{C})} = 125{,}000\ \Omega$$

Choose next larger available size $= 500{,}000\,\Omega$

The current–time characteristics of a thermistor are important in any dynamic analysis of the system. When a step change in voltage is applied to a series circuit consisting of a resistor and a thermistor, a current flows. The time delay for the current to reach its maximal value is a function of the voltage applied, the mass of the thermistor, and the value of the series-circuit resistance. Time delays from milliseconds to several minutes are possible with thermistor circuits. Similar time delays occur when the temperature surrounding the thermistor is changed in a step fashion.

Various circuit schemes for linearizing the resistance-versus-temperature characteristics of thermistors have been proposed (Cobbold, 1974; Doebelin, 1990). Modern instruments use microcomputers to correct for nonlinearities, rather than the former circuit schemes.

The circuitry used for thermistor readout is essentially the same as for conductive sensors, and many of the same techniques apply. Bridge circuits give high sensitivity and good accuracy. The bridge circuit shown in Figure 2.2(b) could be used with $R_3 = R_t$ and $R_4 =$ the thermistor resistance at the midscale value.

Very small differences in temperature can be found using a differential-temperature bridge. It is often necessary to measure such minute differences in biological work. An example is the need to determine the temperature difference between two organs or between multiple sites in the same organ.

artery occlusions, and so forth) (Qi, 2006). Here we shall deal with the basic principles of thermal radiation and detector systems.

Every body that is above absolute zero radiates electromagnetic power, the amount being dependent on the body's temperature and physical properties. For objects at room temperature, the spectrum is predominantly in the far- and extreme-far-infrared regions.

A blackbody is an ideal thermal radiator; as such, it absorbs all incident radiation and emits the maximal possible thermal radiation. The radiation emitted from a body is given by Planck's law multiplied by emissivity ε. This expression relates the radiant flux per unit area per unit wavelength W_λ at a wavelength λ (μm) and is stated as

$$W_\lambda = \frac{\varepsilon C_1}{\lambda^5 (e^{C_2/\lambda T} - 1)} \quad (\text{W/cm}^2 \cdot \mu\text{m}) \tag{2.25}$$

where

$C_1 = 3.74 \times 100$ ($\text{W} \cdot \mu\text{m}^4/\text{cm}^2$)

$C_2 = 1.44 \times 10^4$ ($\mu\text{m} \cdot \text{K}$)

T = blackbody temperature, K

ε = emissivity, the extent by which a surface deviates from a blackbody ($\varepsilon = 1$)

Figure 2.16(a) shows a plot of (2.25), the spectral radiant emittance versus wavelength for a blackbody at 300 K.

Wien's displacement law gives the wavelength λ_m for which W_λ is a maximum. It can simply be found by differentiating (2.25) and setting this to zero.

$$\lambda_m = \frac{2898}{T} \quad (\mu\text{m}) \tag{2.26}$$

Figure 2.16(a) indicates $\lambda_m = 9.66\,\mu\text{m}$ ($T = 300\,\text{K}$). Note from (2.25) that the maximal level of spectral emittance increases with T, and from (2.26) that λ_m is inversely related to T.

The total radiant power W_t, can be found by integrating the area under the curve. This expression is known as the *Stefan–Boltzmann law*.

$$W_t = \varepsilon \sigma T^4 \quad (\text{W/cm}^2) \tag{2.27}$$

where σ is the Stefan–Boltzmann constant (see Appendix).

It is of interest to examine how the percentage of total radiant power varies with wavelength for room-temperature objects. This parameter, plotted in Figure 2.14(a), is found by dividing $\int_0^\lambda W_\lambda d\lambda$ by the total radiant power W, (2.27). Note that approximately 80% of the total radiant power is found in the wavelength band from 4 to 25 μm.

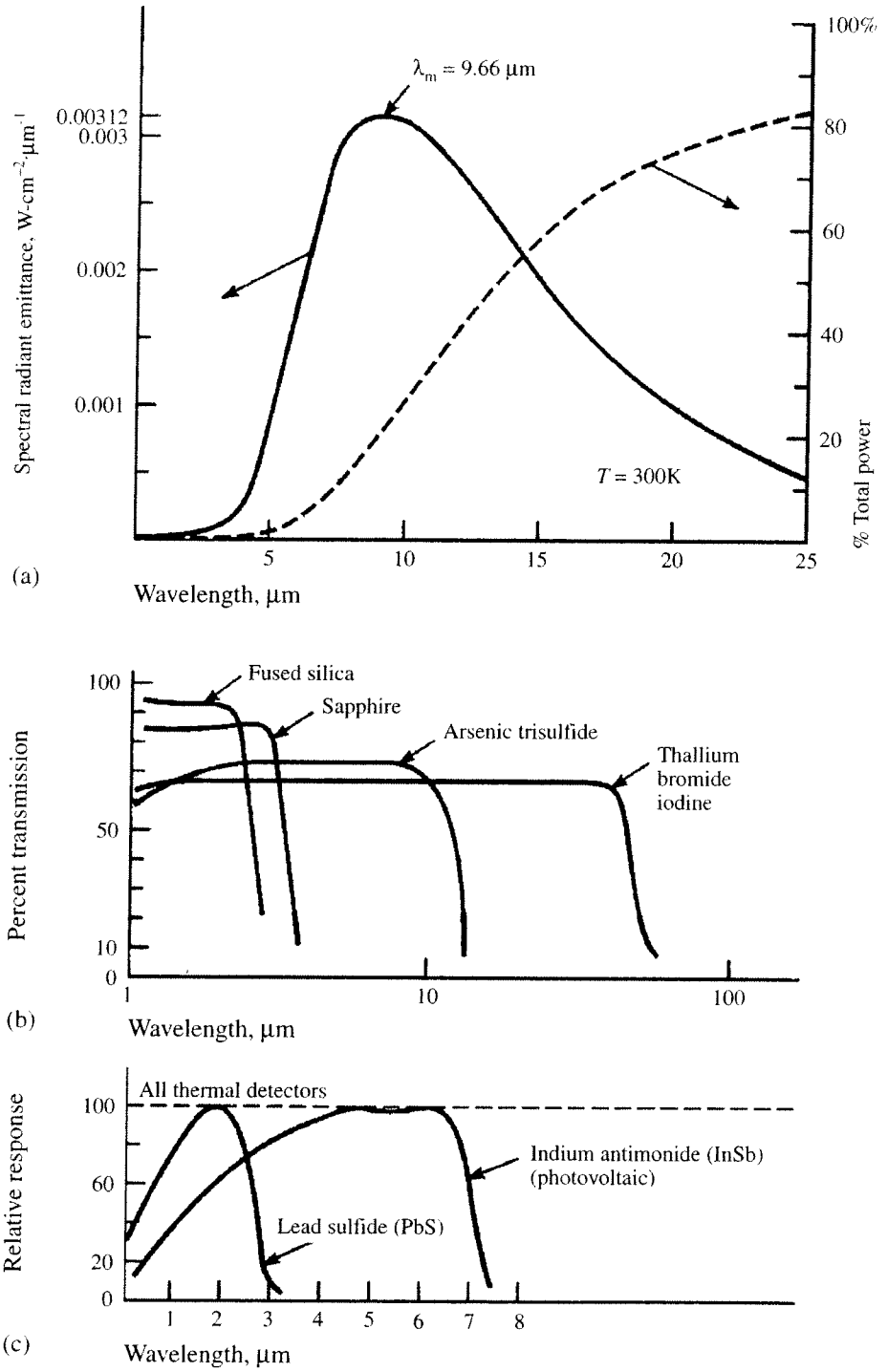

Figure 2.16 (a) Spectral radiant emittance versus wavelength for a blackbody at 300 K on the left vertical axis; percentage of total energy on the right vertical axis. (b) Spectral transmission for a number of optical materials. (c) Spectral sensitivity of photon and thermal detectors. [Part (a) is from *Transducers for Biomedical Measurements: Principles and Applications*, R. S. C. Cobbold. Copyright © 1974, John Wiley & Sons, Inc. Reprinted by permission of John Wiley & Sons, Inc. Parts (b) and (c) are from *Measurement Systems: Application and Design*, E. O. Doebelin. Copyright © 1990 by McGraw-Hill, Inc. Used with permission of McGraw-Hill Book Co.]

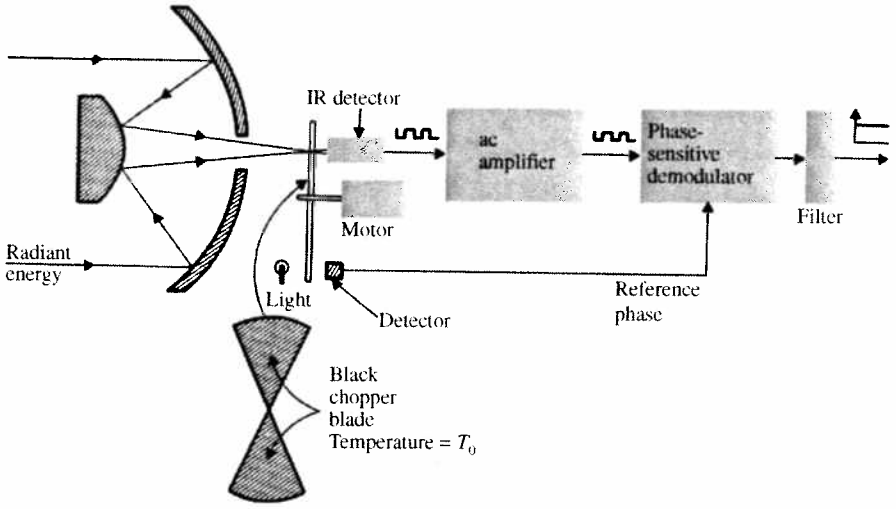

Figure 2.17 Stationary chopped-beam radiation thermometer (From *Transducers for Biomedical Measurements: Principles and Applications,* by R. S. C. Cobbold. Copyright (c) 1974, John Wiley and Sons, Inc. Reprinted by permission of John Wiley and Sons, Inc.)

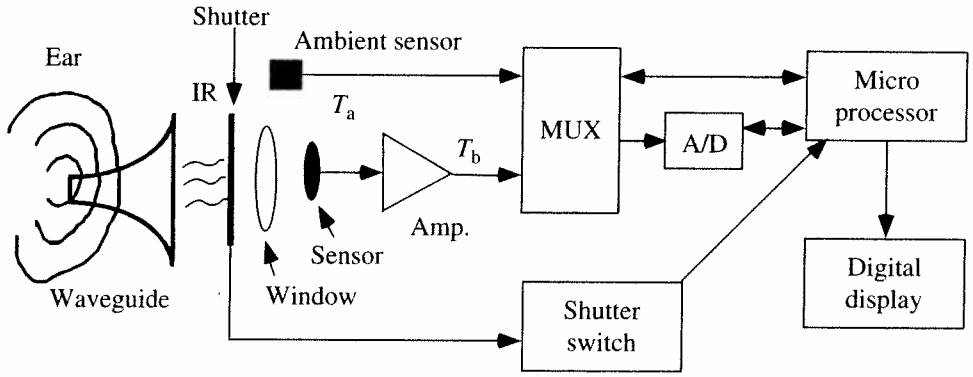

Figure 2.18 The infrared thermometer opens a shutter to expose the sensor to radiation from the tympanic membrane. [From J. G. Webster (ed.), *Bioinstrumentation*, New York: John Wiley & Sons, 2004.]

body's main thermostat, which regulates the core body temperature. This approach has advantages over using mercury thermometers, thermocouples, or thermistors. The standard temperature-measuring techniques measure the temperature of the sensor, not that of the subject. The sensor must be in contact with the patient long enough for its temperature to become the same as, or close to, that of the subject whose temperature is being measured. However, the infrared thermometry device detects emitted energy that is proportional to the actual temperature of the subject. There is negligible thermal time constant for the pyroelectric sensor (Fraden, 1997). The infrared tympanic temperature-monitoring system has a response time in the order of 0.1 s and an accuracy of approximately 0.1 °C. A disposable sanitary probe cover is used to prevent cross-contamination from patient to patient. Ear thermometry offers several clinical benefits over taking sublingual (oral) or rectal measurements. Response is rapid, and readings can be obtained

independent of user technique and degree of patient activity or cooperation (Fraden, 1991).

Infrared tympanic temperature-monitoring systems require a calibration target in order to maintain their high accuracy.

2.11 FIBER-OPTIC TEMPERATURE SENSORS

Figure 2.19 shows the details of a GaAs semiconductor temperature probe (Samaras, 2006). A small prism-shaped sample of single-crystal undoped GaAs is epoxied at the ends of two side-by-side optical fibers. The sensors and fibers can be quite small, compatible with biological implantation after being sheathed. One fiber transmits light from a light-emitting diode source to the sensor, where it is passed through the GaAs and collected by the other fiber for detection in the readout instrument. Some of the optical power traveling through the semiconductor is absorbed, by the process of raising valence-band electrons, across the forbidden energy gap into the conduction band. Because the forbidden energy gap is a sensitive function of the material's temperature, the amount of power absorbed increases with temperature.

This nonmetallic probe is particularly suited for temperature measurement in the strong electromagnetic heating fields used in heating tissue for cancer therapy or in patient rewarming.

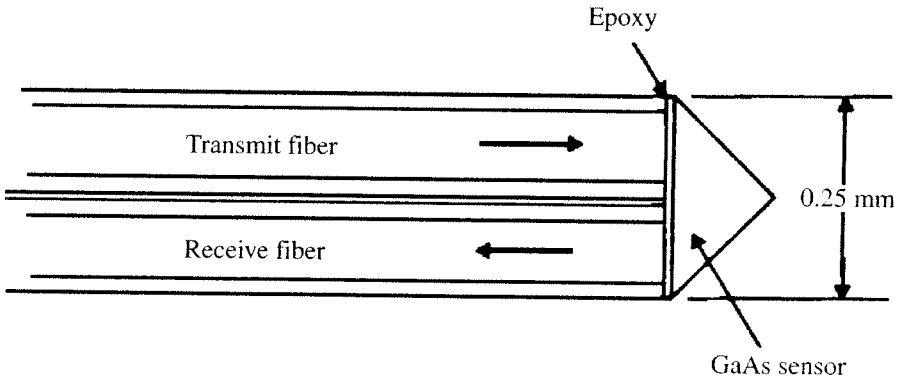

Figure 2.19 Details of the fiber-sensor arrangement for the GaAs semiconductor temperature probe.

2.12 OPTICAL MEASUREMENTS

Optical systems are widely used in medical diagnosis. The most common use occurs in the clinical-chemistry lab, in which technicians analyze samples of blood and other tissues removed from the body. Optical instruments are also used during cardiac catheterization to measure the oxygen saturation of hemoglobin and to measure cardiac output.

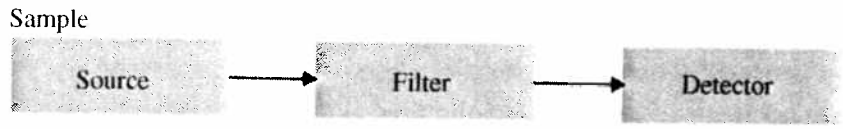

(a)

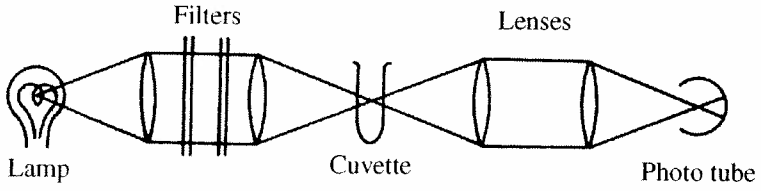

(b)

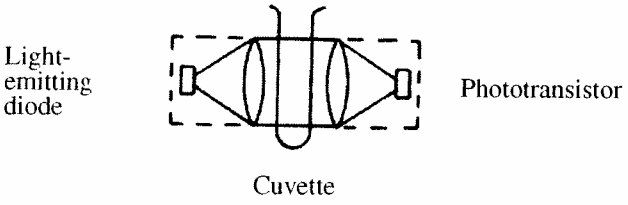

(c)

Figure 2.20 (a) General block diagram of an optical instrument. (b) Highest efficiency is obtained by using an intense lamp and lenses to gather and focus the light on the sample in the cuvette, and a sensitive detector. (c) Solid-state lamps and detectors may simplify the system.

Figure 2.20(a) shows that the usual optical instrument has a source, filter, and detector. Figure 2.20(b) shows a common arrangement of components. Figure 2.20(c) shows that in some cases, the function of source, filter, sample, and detector may be accomplished by solid-state components.

The remainder of this chapter is divided into sections that deal with sources, geometrical optics, filters, detectors, and combinations thereof.

2.13 RADIATION SOURCES

TUNGSTEN LAMPS

Incandescent tungsten-wire filament lamps are the most commonly used sources of radiation. Their radiant output varies with temperature and wavelength, as given by (2.25). For $\lambda < 1\ \mu m$, tungsten has an emissivity of about 0.4 and thus emits about 40% of what it would if the emissivity were 1.0. The relative-output spectrum shown in Figure 2.21(a) is only slightly altered. For higher temperatures, λ_m, the maximal wavelength of the radiant-output

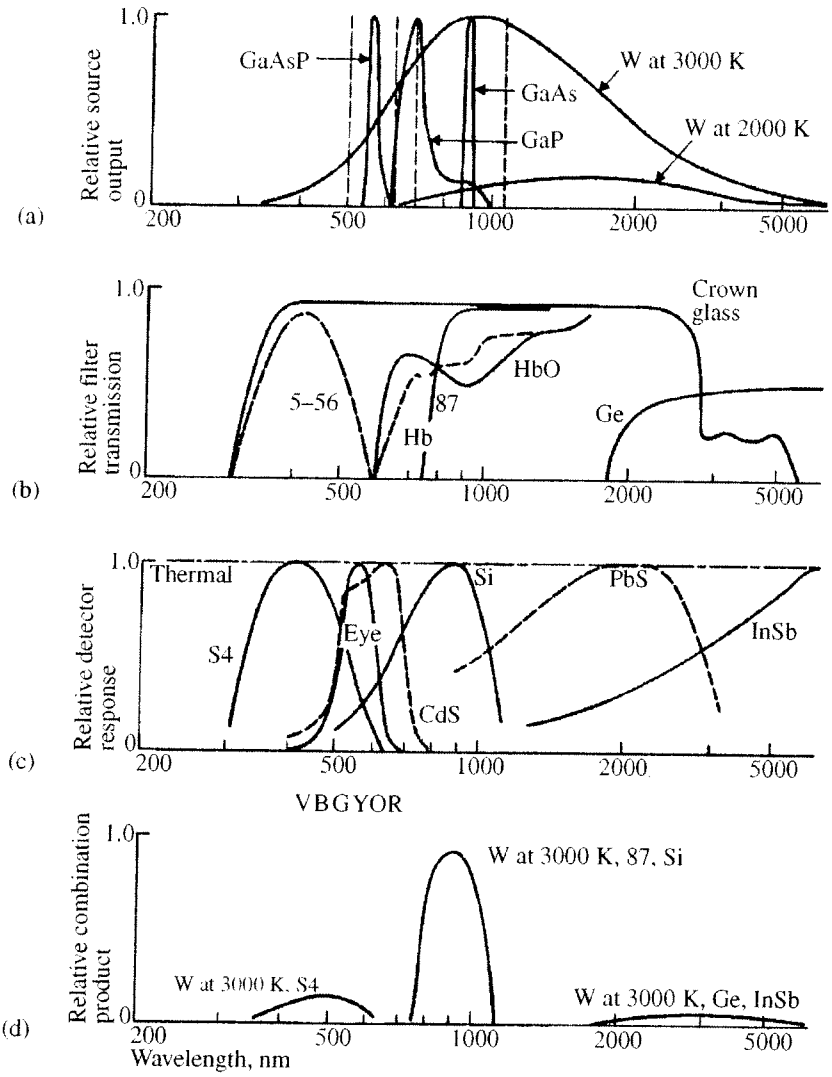

Figure 2.21 Spectral characteristics of sources, filters, detectors, and combinations thereof (a) Light sources: tungsten (W) at 3000 K has a broad spectral output. At 2000 K, output is lower at all wavelengths and peak output shifts to longer wavelengths. Light-emitting diodes yield a narrow spectral output with GaAs in the infrared, GaP in the red, and GaAsP in the green. Monochromatic outputs from common lasers are shown by dashed lines: Ar, 515 nm; HeNe, 633 nm; ruby, 693 nm; Nd, 1064 nm; CO_2 (not shown), 10,600 nm. (b) Filters: A Corning 5-56 glass filter passes a blue wavelength band. A Kodak 87 gelatin filter passes infrared and blocks visible wavelengths. Germanium lenses pass long wavelengths that cannot be passed by glass. Hemoglobin Hb and oxyhemoglobin HbO pass equally at 805 nm and have maximal difference at 660 nm. (c) Detectors: The S4 response is a typical phototube response. The eye has a relatively narrow response, with colors indicated by VBGYOR. CdS plus a filter has a response that closely matches that of the eye. Si *p–n* junctions are widely used. PbS is a sensitive infrared detector. InSb is useful in far infrared. *Note*: These are only relative responses. Peak responses of different detectors differ by 10^7. (d) Combination: Indicated curves from (a), (b), and (c) are multiplied at each wavelength to yield (d), which shows how well source, filter, and detector are matched. (e) Photon energy: If it is less than 1 eV, it is

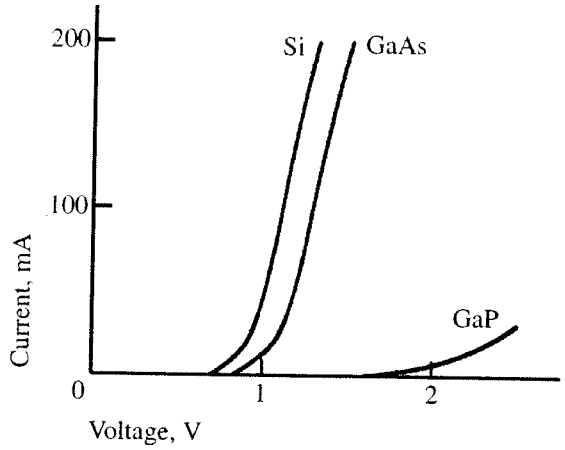

Figure 2.22 Forward characteristics for *p–n* junctions. Ordinary silicon diodes have a band gap of 1.1 eV and are inefficient radiators in the near-infrared range. GaAs has a band gap of 1.44 eV and radiates at 900 nm. GaP has a band gap of 2.26 eV and radiates at 700 nm.

LIGHT-EMITTING DIODES (LEDS)

Light-emitting diodes are *p–n* junction devices that are optimized for radiant output. The ordinary silicon *p–n* junction characteristic shown in Figure 2.22 emits radiant power when a current (typically 20 mA) passes in the forward direction. Spontaneous recombination of injected hole and electron pairs results in the emission of radiation. Because the silicon band gap is 1.1 eV, the wavelength is at about 1100 nm. The silicon device is not efficient. However, GaAs has a slightly higher band gap, as shown in Figure 2.22, and therefore radiates at 900 nm, as shown in Figure 2.21(a). Although the output is not visible, the efficiency is high and the GaAs device is widely used. It can be switched in less than 10 ns.

Figure 2.21(c) and Figure 2.21(e) show that, in order to produce visible light, the band gap of a *p–n* junction must exceed 1.9 eV. The GaP LED in Figure 2.22 has a band gap of 2.26 eV, requires a larger forward-bias voltage than silicon diodes, and is electroluminescent at 700 nm, as shown in Figure 2.21(a). It is an efficient visible LED and produces a bright red light. The GaAsP LEDs make use of a special phosphor that absorbs two photons at one wavelength and emits a single photon at a shorter wavelength. The GaAs is Si doped to emit radiation at 940 nm. Power at this wavelength is absorbed by the phosphor coating that emits green light at 540 nm, as shown in Figure 2.21(a). The decay time of the phosphor is about 1 ms.

Light-emitting diodes are compact, rugged, economical, and nearly monochromatic. They are widely used in a variety of medical, transportation, and industrial circuits. A variety of circuits are available for LEDs and photodetectors using either steady or modulated radiation.

LASERS

Laser (light amplification by stimulated emission of radiation) action can occur in GaAs. The end faces that are perpendicular to the *p–n* junction are polished

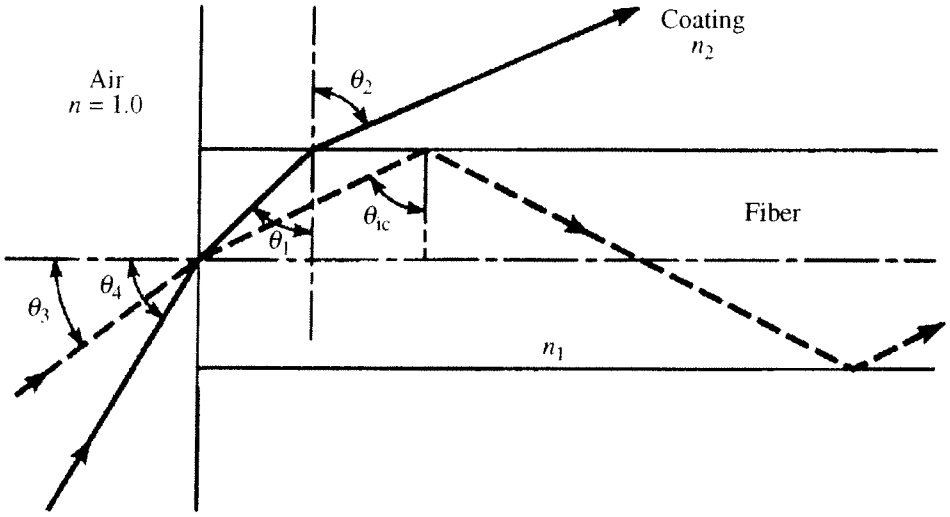

Figure 2.23 Fiber optics The solid line shows refraction of rays that escape through the wall of the fiber. The dashed line shows total internal reflection within a fiber.

Fiber-optic (FO) sensors are replacing some conventional sensors for measuring a variety of electrical, electronic, mechanical, pneumatic, and hydraulic variables (Sirohi and Kothiyal, 1991; Udd, 1991). They are chemically inert and have freedom from electromagnetic interference.

A 50 cm glass fiber exhibits a transmission exceeding 60% for wavelengths between 400 and 1200 nm. A 50 cm plastic fiber has a transmission exceeding 70% for wavelengths between 500 and 850 nm. Although a single fiber is useful for sampling incident radiation of a small area, most applications use flexible bundles of about 400 fibers. In *noncoherent bundles* (called *light guides*), the diameter of a fiber is typically 13 to 100 nm. There is no correlation between a fiber's spatial position at the input and at the output. These fibers are useful only for transmitting radiation. In one application, light is transmitted through the flexible bundle for viewing internal organs (Northrop, 2002). In a second application, an instrument that measures blood oxygen saturation within the vessels alternately transmits radiation at two wavelengths down one bundle (Chapter 10). The radiation is backscattered by the red-blood cells and returned to the instrument for analysis through a second bundle.

In *coherent-fiber bundles*, the fibers occupy the same relative position at both end faces. An image at one end is faithfully transmitted to the other end. The most important medical application of these fibers is in the *endoscope* (a tube for examining body cavities through natural openings) (Hooper, 2006). A typical endoscope is 1 m long and 1 cm in diameter and may be used for viewing the lining of the stomach, intestines, and so forth. A noncoherent bundle transmits light for illumination. A small lens focuses the image of the lining onto the end of a coherent bundle, which transmits the image in such a way that it may be viewed or photographed. External levers make it possible to steer the internal end of the optical-fiber device over a 360° range so that the examining physician can look at cavity walls and around corners.

PHOTOEMISSIVE SENSORS

Photoemissive sensors—an example is the *phototube*—have photocathodes coated with alkali metals. If the energy of the photons of the incoming radiation is sufficient to overcome the work function of the photocathode, the forces that bind electrons to the photocathode are overcome, and it emits electrons. Electrons are attracted to a more positive anode and form a current that is measured by an external circuit. Photon energies below 1 eV are not large enough to overcome the work function, so wavelengths longer than 1200 nm cannot be detected. Figure 2.21(c) shows the spectral response of the most common photocathode, the S4, which has lower sensitivity in the ultraviolet region because of absorption of radiation in the glass envelope.

The *photomultiplier* shown in Figure 2.24 is a phototube combined with an electron multiplier (Lion, 1975). Each accelerated electron hits the first dynode with enough energy to liberate several electrons by secondary emission. These electrons are accelerated to the second dynode, where the process is repeated, and so on. Time response is less than 10 ns. Photomultipliers are the most sensitive photodetectors. When they are cooled (to prevent electrons from being thermally generated), they can count individual photons. The eye is almost as sensitive; under the most favorable conditions, it can detect six photons arriving in a small area within 100 ms. Photodiodes have replaced photomultipliers in many applications.

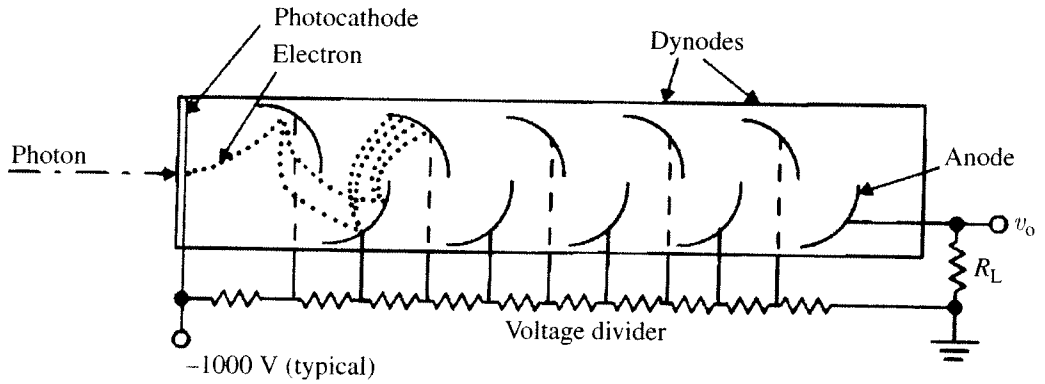

Figure 2.24 Photomultiplier An incoming photon strikes the photocathode and liberates an electron. This electron is accelerated toward the first dynode, which is 100 V more positive than the cathode. The impact liberates several electrons by secondary emission. They are accelerated toward the second dynode, which is 100 V more positive than the first dynode. This electron multiplication continues until it reaches the anode, where currents of about 1 μA flow through R_L.

PHOTOCONDUCTIVE CELLS

Photoresistors are the simplest solid-state photoelectric sensors. A photosensitive crystalline material such as CdS or PbS [Figure 2.21(c)] is deposited

on a ceramic substrate, and ohmic electrodes are attached. If a photon of the incoming radiation has sufficient energy to jump the band gap, hole–electron pairs are produced because the electron is raised from the valence band to the conduction band. The presence of the electrons in the conduction band and of the holes in the valence band increases the conductivity of the crystalline material so that the resistance decreases with input radiation. Photocurrent is linear at low levels of radiation but nonlinear at levels that are normally used. It is independent of the polarity of applied voltage. After a step increase or decrease of radiation, the photocurrent response rises and decays with a time constant of from 10 to 0.01 s, depending on whether the radiation is low or high.

PHOTOJUNCTION SENSORS

Photojunction sensors are formed from *p–n* junctions and are usually made of silicon. If a photon has sufficient energy to jump the band gap, hole–electron pairs are produced that modify the junction characteristics, as shown in Figure 2.25. If the junction is reverse-biased, the reverse photocurrent flowing from the cathode to the anode increases linearly with an increase in radiation. The resulting photodiode responds in about 1 μs. In phototransistors, the base lead is not connected, and the resulting radiation-generated base current is multiplied by the current gain (beta) of the transistor to yield a large current from collector to emitter. The radiation–current characteristics have a nonlinearity of about 2% because beta varies with collector current. The response time is about 10 μs.

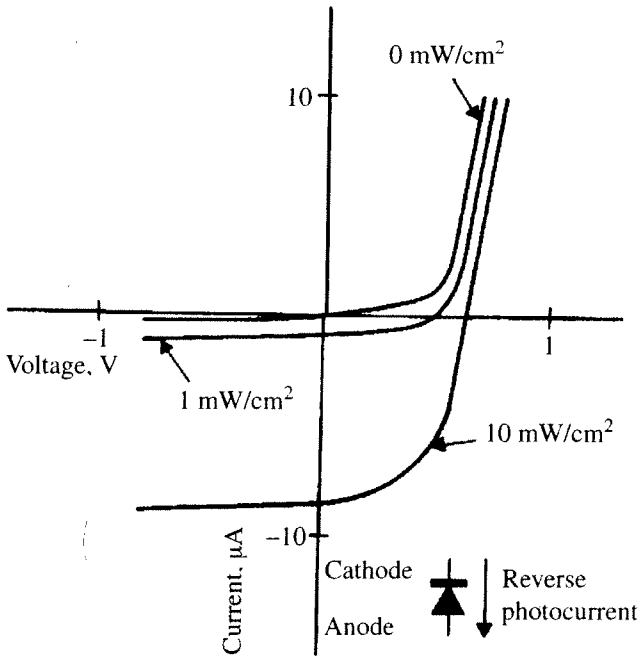

Figure 2.25 Voltage–current characteristics of irradiated silicon *p–n* junction
For 0 irradiance, both forward and reverse characteristics are normal. For 1 mW/cm², open-circuit voltage is 500 mV, and short-circuit current is 0.8 μA. For 10 mW/cm², open-circuit voltage is 600 mV, and short-circuit current is 8 μA.

Silicon p–n junctions are also manufactured as photo Darlington transistors, photo FETs, photo unijunction transistors, and photo silicon-controlled rectifiers (SCRs). Photon couplers are LED–photodiode combinations that are used for isolating electric circuits. For example, they are used for breaking ground loops and for preventing dangerous levels of current from leaking out of equipment and entering the heart of a patient (Section 14.9). Modern photojunction sensors have become so sensitive and with rapid response times so that in many applications they have replaced photomultipliers.

PHOTOVOLTAIC SENSORS

The same silicon p–n junction can be used in the photovoltaic mode. Figure 2.25 shows that there is an open-circuit voltage when the junction receives radiation. The voltage rises logarithmically from 100 to 500 mV as the input radiation increases by a factor of 104. This is the principle of the solar cell that is used for direct conversion of the sun's radiation into electric power.

SPECTRAL RESPONSE

All of the aforementioned silicon sensors have the spectral response shown in Figure 2.21(c). There is no response above 1100 nm because the energy of the photons is too low to permit them to jump the band gap. For wavelengths shorter than 900 nm, the response drops off because there are fewer, more-energetic photons per watt. Each photon generates only one hole–electron pair.

Because none of the common sensors is capable of measuring the radiation emitted by the skin (300 K), which has a peak output at 9000 nm, special sensors have been developed, such as the InSb sensor shown in Figure 2.21(c).

2.17 OPTICAL COMBINATIONS

In order to specify the combinations of sources, filters, and sensors, instrument designers require radiometric units that must be weighted according to the response curve of each element. The total effective irradiance, E_e, is found by breaking up the spectral curves into many narrow bands and then multiplying each together and adding the resulting increments (Stimson, 1974). Thus

$$E_e = \sum S_\lambda F_\lambda D_\lambda \Delta\lambda \tag{2.30}$$

where

S_λ = relative source output

F_λ = relative filter transmission

D_λ = relative sensor responsivity